Experimental Verification and Full-Scale Deployment of Global Positioning Systems to Monitor the Dynamic Response of Tall Buildings

T. Kijewski-Correa, M.ASCE[1]; A. Kareem, M.ASCE[2]; and M. Kochly, S.M.ASCE[3]

Abstract: The Civil Engineering community has long needed methods of accurate global displacement measurement for use in construction and more recently in the areas of structural health monitoring. Global Positioning Systems (GPS) provide one answer to this challenge, with rapid advancements in the available sampling rates and tracking resolution. However, as a relatively new dynamic sensing technology, GPS performance must be thoroughly validated before its application in full scale. This paper details an experimental program with this aim, documenting the performance of a high-precision GPS in terms of its background noise and dynamic tracking ability, while providing position quality thresholds suitable for qualifying the accuracy of tracking in full scale. Given the performance observed in these studies, considerations for full-scale deployment are offered as well as an assessment of its efficacy in monitoring the dynamic motions of a tall building through the Chicago full-scale monitoring project.

DOI: 10.1061/(ASCE)0733-9445(2006)132:8(1242)

CE Database subject headings: Displacement; Measurement; Structural reliability; Global positioning; Buildings, high-rise; Dynamic response.

Introduction

With the growing complexity and cost of Civil Engineering projects, there is significant interest in securing that investment on two fronts: first in the safe operation and maintenance of the project to ensure a long service life and second in insuring safety and efficiency of modern design practice. Both of these intentions can benefit from instrumentation and monitoring of the structure, whether it is at the global level, using accelerometers, or at a local level using strain sensing elements. However, monitoring the global response via accelerometers, though well established, can only provide an indication of resonant response and fails to capture static and quasi-static behaviors. In the context of health monitoring, static deflections, whether due to settlement, thermal expansions, or even permanent damage following some unforeseen event, are equally important quantities of interest. Particularly, in the context of tall, flexible structures, such static and quasi-static response contributions can be significant and are rarely observed in full scale due to the customary use of accelerometers.

[1]Rooney Family Assistant Professor, Dept. of Civil Engineering and Geological Sciences, Univ. of Notre Dame, 156 Fitzpatrick Hall, Notre Dame, IN 46556 (corresponding author). E-mail: tkijewsk@nd.edu

[2]Robert M. Moran Professor, Univ. of Notre Dame, 156 Fitzpatrick Hall, Notre Dame, IN 46556. E-mail: kareem@nd.edu

[3]Graduate Student, Univ. of Notre Dame, 156 Fitzpatrick Hall, Notre Dame, IN 46556. E-mail: mkochly@nd.edu

Note. Associate Editor: Ahmet Emin Aktan. Discussion open until January 1, 2007. Separate discussions must be submitted for individual papers. To extend the closing date by one month, a written request must be filed with the ASCE Managing Editor. The manuscript for this paper was submitted for review and possible publication on April 14, 2005; approved on October 10, 2005. This paper is part of the ***Journal of Structural Engineering***, Vol. 132, No. 8, August 1, 2006. ©ASCE, ISSN 0733-9445/2006/8-1242–1253/$25.00.

Methods of global displacement sensing were subsequently developed in response to these needs. Techniques including terrestrial positioning systems, laser displacement sensors, and photo/video imaging techniques have all received recent attention, but have limited utility under inclement atmospheric conditions and are often not feasible for continuous, unattended, long-term monitoring. At the same, military-grade global positioning systems (GPS) were transitioning into the private sector and with rapid advancements in hardware and software, were poised to offer subcentimeter tracking on two orthogonal axes (and vertically with lesser accuracy) at sampling rates of up to 20 Hz continuously, unattended, and in real time.

GPS Theory

While space will not permit an extensive development of GPS theory (readers are referred to more detailed discussions in Kijewski-Correa 2003 or Seeber 1993), some basic elements of the sensing philosophy are now provided to highlight primary error sources. The GPS satellite arrays were established by the Department of Defense and are organized into six orbital planes intended to provide a minimum of 4–5 satellites orbiting at least 15° above the horizon at any location at all times, though 6–8 satellites are typically in view for most users. GPS positions are calculated using the concept of triangulation, using the known position of satellites overhead to determine the position of a GPS receiver/antenna pair on Earth (Fig. 1). Each satellite continuously transmits the current time (kept by atomic clocks), as well as information about its current position (x_i, y_i, z_i) in its orbital path. The distance, or *slant range* (S_i), of the ith satellite to the unknown position on Earth (x, y, z) is determined from the travel time of the transmitted electromagnetic signals (moving at a rate of 290,000 km/s). This position (x, y, z) is defined in terms of the World Geodetic System 1984 (WGS84) coordinate system, which provides, in Cartesian coordinates, the position on the surface of

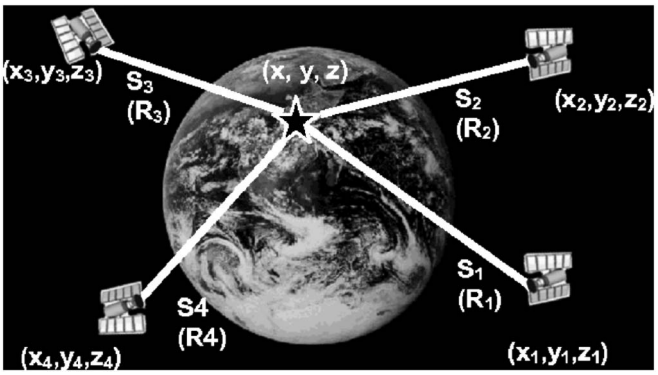

Fig. 1. GPS triangulation concept

an ellipsoid representative of the Earth, as described in Leica (1999a). This can then be projected onto a local coordinate system predefined for every region of the United States. For a constellation of N_{sat} satellites, a series of slant ranges can be defined as

$$S_i = \sqrt{(x_i - x)^2 + (y_i - y)^2 + (z_i - z)^2} \quad i = 1,2, \ldots N_{sat} \qquad (1)$$

By inspection, a minimum of three satellites would be required to determine a position estimate, however, this requires very accurate timing mechanisms (nanosecond-level accuracy) too expensive for civilian GPS receivers. Instead, less accurate quartz crystal clocks are used to determine *psuedoranges* based on uncorrected time values. To account for clock inaccuracies, a time bias b is then introduced into Eq. (1), where slant range is replaced more appropriately by pseudorange, R_i, resulting in

$$R_i = \sqrt{(x_i - x)^2 + (y_i - y)^2 + (z_i - z)^2} - b \quad i = 1,2, \ldots N_{sat} \quad (2)$$

expanding the number of required satellites to a minimum of four to solve for all the system unknowns. It should also be noted that although each satellite has its own atomic clock, the time bias for all is the same as it is defined with respect to the same receiver clock. Typically, as more than four satellites are available, an overdetermined set of equations can be generated using Eq. (2) to obtain an even more accurate position for the receiver.

The transmission of GPS signals over great distances leaves this approach vulnerable to a variety of errors that can slow the rate of transmission and introduce errors into pseudorange estimates. These are primarily the result of disturbances in the upper (ionosphere) and lower (troposphere) atmosphere. As signals in the ionosphere slow at a rate proportional to their frequency, an estimate of ionospheric delay can be made by tracking both of the navigation messages transmitted by GPS on carrier waves at the *L*-band frequencies of 1.57542 GHz (*L*1) and 1.22760 GHz (*L*2) through so-called *dual frequency* GPS units. The troposheric delays are associated with local weather fluctuations that limit the position accuracy of an autonomous GPS receiver to the order of meters. However, by establishing a stationary checkpoint or *reference* receiver with known position in the general locale of the receiver used for position tracking (termed the *rover*), these troposheric errors can be eliminated. This forms the basis for differential GPS (DGPS) tracking, where the overall accuracy is proportional to the baseline separation between the rover and reference and is on the order of centimeters or even millimeters. In the real-time kinematic (RTK) configuration, these position corrections from the reference are transmitted continuously by radio or high-speed internet link.

Even with these corrections, accuracy of GPS tracking depends not only on the number of satellites visible but also on their position overhead, given the reliance on the surveying concept of resection. Position tracking is enhanced when the satellites used in Eq. (2) are well spaced, i.e., ideally three satellites spaced 120° in plane with a fourth satellite directly overhead. The deviation from this idealized configuration is quantified by the dilution of precision (DOP) markers issued by the GPS receiver, which fluctuate continuously throughout the day as satellite constellations change overhead. For example, the position DOP (PDOP) should be kept under 3 for high-accuracy tracking. Aside from degradations in tracking quality due to satellite positions, the other primary concern for GPS tracking, particularly in urban zones, is the multipath effect (Axelrad et al. 1996). This error is the result of a satellite signal being reflected off of one or more objects and, having a longer path, arriving at the receiver with a slight delay. Their processing in conjunction with the directly received version of the signal leads to long-period distortions in position estimates that repeat themselves each sidereal day (23 h, 56 min) as the satellites repeat their orbits. This was documented in one of the first applications of GPS to monitor tall, flexible structures by Lovse et al. (1995) in their work on the Calgary Tower. Provisions to mitigate this effect include the use of choke ring antennas (Tranquilla et al. 1994; Counselman 1999), off-line filtering (Chen et al. 2001; Kochly et al. 2005), and embedded receiver algorithms (Van Nee 1995; Leica 1999b).

Full-Scale Monitoring of Buildings by GPS

The applications of GPS to surveying and monitoring of static and pseudostatic motions of land masses, dams, and bridges are quite extensive and cannot be chronicled here. As the intent of this work is to highlight the application of the technology in urban zones for the monitoring building structures, only those applications shall now be summarized. The instrumentation of mid- to high-rise buildings, in addition to the application presented here, include 34- and 44-story buildings in California (Celebi 2000; Celebi and Sanli 2002), short-term deployments on the Di Wang building (384 m, China) (Guo and Ge 1997; Chen et al. 2001), Republic Plaza (280 m, Singapore) (Brownjohn 2003), and a 66-story building in Korea (Park et al. 2004).

Calibration Program

Most of the aforementioned full-scale deployments of GPS were not preceded by detailed calibration studies. However, given the relative infancy of this technology, the authors embarked on an extensive calibration program in 2002, which is presented here to document the capabilities of the sensor, building upon the earlier validation efforts of Celebi (2000) using flexible beams and Tamura et al. (2002), who performed sinusoidal calibration studies using a mechanical shaker. These efforts have been recently followed by impulse response testing of a flexible model (Park et al. 2004) and biaxial motion simulator calibrations (Chan et al. 2005). Again, readers are referred to Kijewski and Kareem (2002) and Kijewski-Correa (2003) for a more detailed overview of the calibration program and GPS hardware and software settings.

Table 1. Accuracy Levels for Leica MC 500 in DGPS Configuration

Dynamic accuracy	5.00 mm+2.00 ppm
Static accuracy	3.00 mm+ 0.50 ppm

Note: ppm=parts per million, determined by dividing baseline distance in millimeters by 1,000,000.

GPS Components

The components used in this DGPS calibration program include a pair of Leica MC 500 dual frequency, 12 channel receivers with maximum sampling rate of 10 Hz coupled with International GPS Service, gold anodized choke ring antennas with protective radomes. The antennas incorporate a ground plane and four concentric choke rings to minimize multipath signal reception from low elevation reflected signals. Table 1 lists Leica's reported accuracy levels for a DGPS system employing the hardware described above. It should be noted that with each generation of GPS receivers, there have been considerable improvements in tracking accuracy and new designs are now enabling sampling rates of over 20 Hz. Such advancements in capability, coupled with the anticipated reductions in cost, make this monitoring technology increasingly viable. Though the GPS hardware chosen does have fully RTK capabilities, potential data loss due to wireless communications challenges would prohibit timely and accurate verification of the sensor's capabilities. Thus a post-processing scheme was adopted where positioning data at both the reference and rover installations is recorded directly to the receiver ring buffers on 96 MB personal computer (PC) cards and then transferred to on-site laptops running Leica ControlStation (v. 4.2) software, providing the necessary remote control and communications portal (Fig. 2). The data from the reference and rover on-site PCs could then be downloaded by telephone or Ethernet to an off-site postprocessing PC running Leica SKI-Pro software to determine final position estimates for the rover off line. This configuration also allows user flexibility in changing various postprocessing parameters, e.g., ionospheric model, stochastic model, and tropospheric model, settings that cannot be revisited if the data is processed in real time. SKI-Pro outputs were then translated by transverse mercator projection from the global WGS84 coordinate system and into a local coordinate system for the area (Leica 1999a), allowing displacements to be viewed in terms of their North–South (N-S) and East-West (E–W) components. The postprocessing protocol also included second-order Chebyshev lowpass filtering to remove high frequency noise from the recorded data. An APC Battery BackUp 500 VA uninterruptible power supply was also added to support the system during temporary power losses. Note also in Fig. 2 that the LMR 400 coaxial cabling linking the GPS receiver and antenna was outfitted with a grounded gas capsule (Huber+Suhner 3402.17.K) for in-line lightning protection.

Test Configuration

In order to identify the best possible performance of the system, calibration tests were conducted in an open field location sufficiently free from potential sources of multipath error and from obstructions that may block lower elevation satellites from view. A series of tests were conducted to verify the GPS performance, quantified through the static background noise and the accuracy in dynamic tests, where displacements of the rover antenna were simulated by a portable motion simulator. The GPS antennas were mounted on wooden platforms to avoid blockages during testing, were separated by a 2.5 m baseline, and were oriented so motions

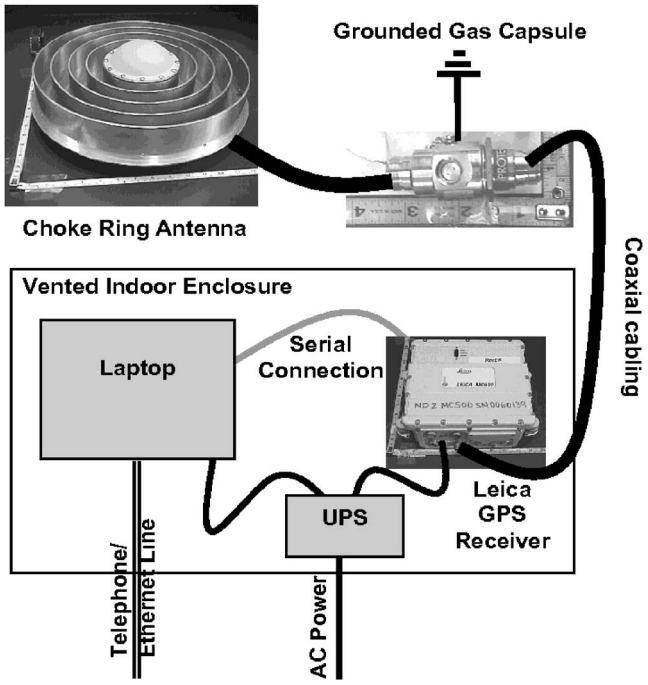

Fig. 2. Schematic configuration of GPS components

of the simulator would be along the N-S direction, as shown in Fig. 3. In this testing program, the physical rotation of the ball screw driving the displacement-controlled motion simulator was taken as the actual displacement of the antenna/mount assembly being tracked at 10 Hz by the rover GPS unit. Prior to each day's testing, each receiver was set to self-survey to establish a baseline condition. Approximately 40 tests were conducted using this configuration to investigate dynamic tracking ability, background noise, influence of in-line surge protection, influence of mount dynamics and corrections for orientations not aligned with true North (Table 2). Though full details of all of these tests are available in Kijewski-Correa (2003), only the former two test series

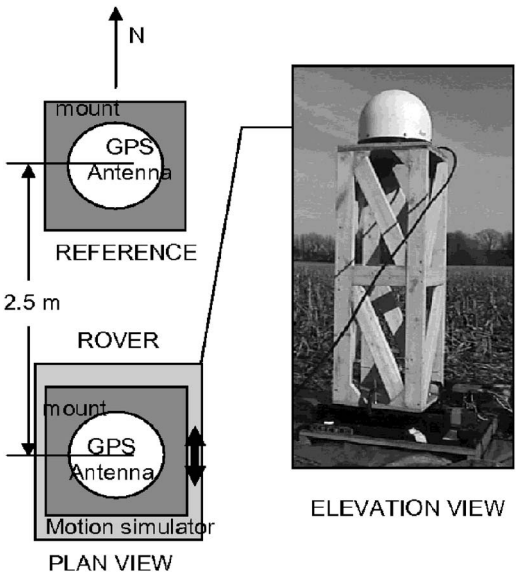

Fig. 3. Schematic of reference and rover antenna orientations for calibration testing

Table 2. Summary of Calibration Tests Conducted

Test	Description	Purpose
1a-d	Static	Background noise, influence of DOP
2a-w	Sine wave: ±0.5–±3.0 cm at 0.1–1 Hz	Tracking ability over varying amplitudes, frequencies
3a	Sinusoidal chirp	Ability to track complex signals
3b	Random noise	Ability to track complex signals
3c-f	Simulated structural responses	Ability to track realistic building motions
4a-c	Static with gas capsule	Determine influence of in-line gas capsule
5	Sine wave: ±2.0 cm at 0.2 Hz	Validate on-site coordinate transformations
6a-b	Static	Determine influence of antenna mount dynamics

are discussed herein. In these tests, relative motions along the N-S axis are defined as ΔN and those along the E-W axis are defined as ΔE.

Verification of Background Noise by Static Testing

Static tests (motion simulator held fixed) were conducted to quantify the background noise in the system, i.e., levels of motion falsely detected when the rover is stationary for a period of 10 min. By conducting these tests throughout the day, the influence of DOP on background noise could also be investigated. As shown in Fig. 4, Tests 1a and 1d demonstrate a classical circular shape, indicating equivalent accuracy levels in both directions. The elliptical form in Tests 1b and 1c indicate biases resulting from the low frequency trends in the GPS data. These figures also display the standard deviations predicted by the manufacturer in comparison to those observed in testing, reiterating that even in the noisiest of the three tests (Test 1c), the RMS of the background noise was within the accuracy limits defined by the manufacturer. In addition to these static tests, during all other tests listed in Table 2, motions along the E-W axis were essentially static given the orientation of the single axis motion simulator. The averaged statistical characteristics of the background noise levels along the E-W axis are summarized in Table 3 to confirm that the unit's performance consistently surpassed manufacturer's expectations throughout the testing program.

An example of the spectral and probabilistic nature of the background noise is provided in Fig. 5, affirming the generally broadband nature of GPS background noise with evidence of the low frequency trends previously noted. The probability density functions reveal the non-Gaussian nature of the background noise, though it can be demonstrated that in the tail regions, the Gaussian distribution provides a conservative measure of the spread of the background noise, capturing the majority of the background noise within in the 99.7% confidence limits (see Table 4). As these extremes are most relevant to the performance of GPS, it can be assumed that a Gaussian description provides a conservative model for the background noise.

In calibration studies such as those presented here, the level of background noise is readily quantified by observing the "static" GPS responses. Unfortunately, in full-scale deployment, motions

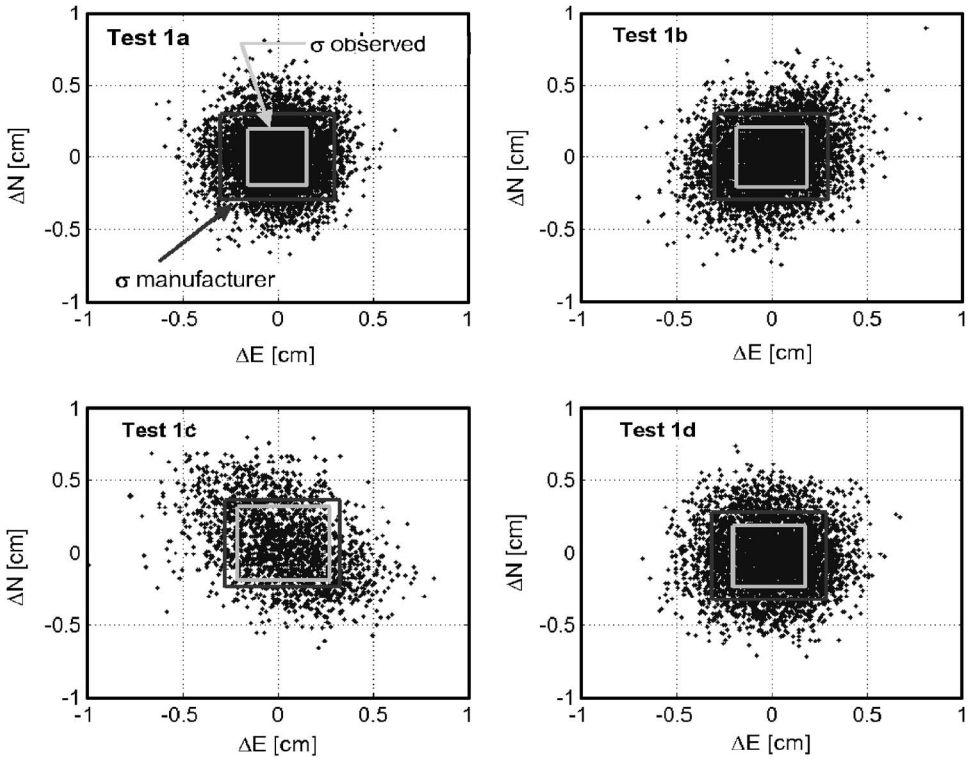

Fig. 4. Results from static tests and comparisons between observed RMS displacement (inner box) and manufacturer's prediction (outer box)

Table 3. Summary of Performance from Static Component (ΔE) of Calibration Tests 2 and 3

Range	±0.71 cm
Mean value	0.00 cm
RMS	0.22 cm

are generally bi-axial, leaving no static response component to quantify the noise levels. However, in the postprocessing regimen, a statistical measure of the accuracy of GPS calculated displacements in the Northerly (σ_N) and Easterly (σ_E) directions is provided at each epoch. Note that in the case of the static tests, it was demonstrated that, using the conservative assumption of a Gaussian distribution, over 99% of the background noise fell within three standard deviations. It is now proposed to use the standard deviation of the position estimates (σ_N and σ_E) provided at each epoch in lieu of estimates of the RMS background noise to provide a time-varying estimate of the sensor's accuracy in full scale. To verify the appropriateness of this assumption, Kijewski-Correa (2003) compared the RMS of the running background noise for each test to the corresponding average of these standard deviations from the GPS solution (σ_N and σ_E). The authors further verified that σ_N and σ_E were not dependent on the motion experienced by the GPS and manifested spectral and statistical similarities to the static test data. As summarized for selected static tests in Table 5, the standard deviations of the GPS position estimates provide a reasonable approximation to the RMS background noise levels observed in static testing. As σ_N and σ_E are available at each epoch, their use in this statistical model will yield a time-varying noise threshold Δ_{noise}, termed by the authors as a position quality threshold (PQT), to quantify the reliability of GPS estimates, according to

$$\Delta_{\text{noise}} = [-3\sigma(t),\ 3\sigma(t)] \tag{3}$$

where $\sigma = \sigma_N$ or σ_E depending on the direction being analyzed. A demonstration of how these constructed thresholds compare to the background noise levels in static testing is provided in Fig. 6 for Test 1a, with additional comparisons made in Kijewski-Correa (2003). By using the formulation in Eq. (3), the PQTs, with the exception of a few spikes, conservatively define the upper and lower limits of the background system noise and thus provide an envelope to the system's inherent noise that can be extended to full-scale applications. It will be subsequently demonstrated that these thresholds can be used to determine the effective "signal-to-noise" ratio for the system.

Table 4. Comparison of 99.7th Percentile Confidence Limits of GPS Background Noise with Those of Gaussian Distribution

	ΔE (cm)		ΔN (cm)	
Test	Actual	Gaussian	Actual	Gaussian
1a	(−0.46, 0.40)	(−0.47, 0.47)	(−0.52, 0.56)	(−0.58, 0.58)
1b	(−0.51, 0.51)	(−0.56, 0.56)	(−0.56, 0.58)	(−0.62, 0.62)
1c	(−0.58, 0.59)	(−0.62, 0.62)	(−0.57, 0.66)	(−0.69, 0.69)

Verification of Amplitude/Frequency Sensitivity in Dynamic Tracking

The next series of tests presented were designed to quantify the range of frequencies and amplitudes that can be successfully tracked by GPS using simulated sinusoidal motions with amplitudes ranging from ±0.5 up to ±3 cm with frequencies of 0.1, 0.125, 0.15, 0.2, 1, and 2 Hz. The primary focus toward low frequency signals was intentional, as they were selected to represent the fundamental sway frequencies common in the buildings that the system is designed to monitor. The upper limits in amplitude and frequency considered were also constrained by limitations in the motion simulator hardware.

As discussed previously, comparisons will be made between the displacements measured by GPS and the physical displacement of the ball screw in the motion simulator. Table 6 lists the standard deviation and peak values of the motion simulator signal (second row in each grouping) and compares these values to the GPS-measured displacements (first row in each grouping), presenting only the results for sinusoids of 0.1, 1, and 2 Hz for brevity. Note that due to hardware limitations, motions could not be simulated at 2 Hz for the 2 and 3 cm amplitude sine waves. The error in the estimate is shown in the third row in each grouping. For additional insights, the mean PQT, the time-varying quantity defined in Eq. (3), is compared to the peak displacement of the table to form an effective peak "signal-to-noise" ratio. This measure is used to determine if the signal being tracked is of sufficient amplitude in comparison with the level of background noise in the system. As space does not permit the graphical evidence of tracking quality to be provided for all simulated sinusoidal tests conducted, selected results are shown in the results matrix in Fig. 7, while the full suite of results is available in Kijewski-Correa (2003). As expected, as the simulated signal's amplitudes fall beneath the superimposed PQTs, the tracking ability diminishes. Note also that the GPS results do manifest a high frequency distortion that may be removed through additional low-pass filtering. Despite the inability of the GPS to capture peak displacements with repeatable accuracy, the RMS of the

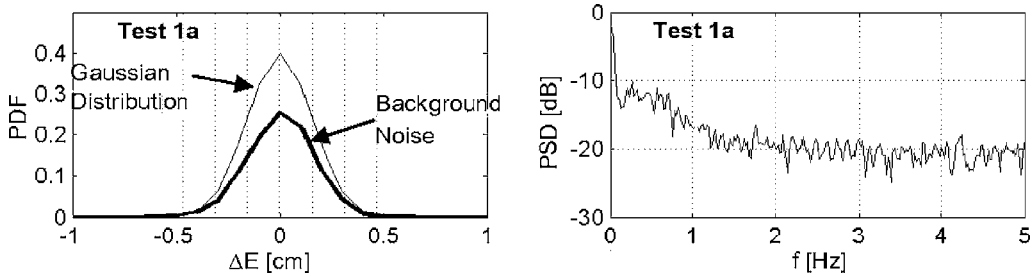

Fig. 5. Probability density (compared to Gaussian distribution with same mean and standard deviation) with vertical bars denoting 1, 2, and 3 SD of mean (left), and power spectral density, both for static Test 1a, ΔE component

Table 5. Standard Deviation of GPS Static Displacements ($\Delta N, \Delta E$) Compared to Average of Standard Deviation in GPS Displacement Solution (σ_N, σ_E) over Monitoring Period

Test	RMS (ΔE)	Avg (σ_E)	RMS (ΔN)	Avg (σ_N)
1a	0.16	0.13	0.19	0.16
1b	0.19	0.13	0.21	0.18
1c	0.21	0.19	0.23	0.20
4a	0.17	0.14	0.30	0.22
4b	0.17	0.16	0.21	0.21
4c	0.20	0.13	0.23	0.17
6a	0.20	0.20	0.28	0.24
6b	0.22	0.22	0.27	0.25

GPS displacements is quite consistent with the RMS of the actual table displacements (within 10%) once the signal-to-noise ratio exceeds 200%, which corresponds roughly to motions above ±1 cm. The findings presented here and in Kijewski-Correa (2003) further indicate that the ability to capture peak values does improve as the amplitude of motion increases, achieving a consistent error of 10% or less when motions are above ±2 cm. These findings demonstrate an improvement over the results in Tamura et al. (2002), who used a previous generation Leica MC 1000 unit. It should also be noted that DOP errors were inherently fluctuating as this sequence of tests was conducted, which will also influence the quality of tracking. It should also be noted that all these calibration studies were conducted for short duration tests. Since GPS constructs its own models to correct for atmospheric delays, the accuracy improves as longer data sets are collected (45 min or more).

Verification of Ability to Track Realistic Building Motions

Though additional tests were conducted using random and chirp signals (Kijewski-Correa, 2003), the authors now present the most relevant test results: the ability of GPS to track the simulated motions of a multidegree of freedom (MDOF) oscillator subjected to zero mean, Gaussian white noise to emulate the wind-induced dynamic response of a flexible building. Two buildings were considered, one with fundamental frequency (f_n) of 0.53 Hz and another with fundamental frequency of 0.12 Hz. Critical damping ratios (ξ) were assumed to be 1% critical. The responses were simulated for a period of 5 min. By varying the system input, two different response levels were generated for each building: 0.53 Hz system with RMS responses of 0.66 and 1.12 cm, and 0.12 Hz system with RMS responses of 1.01 and 1.19 cm. The results of these tests are presented in Table 7 in a format similar to that used in Table 6. Note that the GPS was able to capture peak and RMS responses within 10% error, as expected given the peak signal-to-noise ratios exceeded 200%. Still the system tracked the lower amplitude simulated responses well, as evidenced by Fig. 8, which provides snapshots of 0.12 Hz simulated responses. Note that visual comparisons for all four tests could not be provided for brevity. One explanation for this improved performance is that these tests were of longer duration (5 min) than the sinusoidal test sequence (30 s). The longer duration tests provide the post-processing protocol with more data for atmospheric modeling and thus generally will produce higher quality results. In light of these findings, over longer monitoring periods, both averaged quantities like standard deviation as well as peak measures can be accurately captured within 10% as long as the peak signal amplitude is greater than twice the PQT. As a result, the technology appears to be well-suited for tracking the wind-induced responses of tall, flexible structures.

Full-Scale Deployment

The Chicago full-scale monitoring program (Kareem and Kijewski-Correa 2002) ⟨http://windycity.ce.nd.edu⟩ was established to systematically validate the tools and procedures used in the design of tall buildings by comparing in-situ response values with those predicted by wind tunnel testing and finite element models. This program is being led by the NatHaz Modeling Laboratory at the University of Notre Dame in conjunction with the Boundary Layer Wind Tunnel Laboratory at the University of Western Ontario and Skidmore Owings and Merrill LLP in Chicago, Ill. Through this ongoing monitoring program, three tall buildings in the City of Chicago have been instrumented for a number of years with a data logger system interrogating an array of high-sensitivity force balance accelerometers and ultrasonic anemometers, as discussed in Kijewski-Correa et al. (2006). While the accelerometers that provide the primary instrumentation for the program can capture the resonant response of these buildings in both sway and torsion, they are incapable of providing information on the mean and background components of wind-induced response. It was this underlying factor that motivated the prototyping and calibration of GPS in this study, with the plans of deploying the system on one of the instrumented tall buildings in the program. Note that at the request of building ownership, the identity of the instrumented buildings must remain anonymous at this time. The response sensor array, including GPS and accelerometers, is shown in Fig. 9.

Identification of Reference Site

Following the calibration studies discussed previously, the authors undertook a study of viable reference sites in the Chicago downtown area suitable to achieve millimeter-level tracking in a DGPS configuration. The fact that the reference should be as close to the rover as possible, to minimize the errors discussed in Table 1, precludes the use of traditional reference monuments anchored to the ground, as they would be completely shielded by the surrounding tall buildings in downtown Chicago and thus incapable of tracking satellite transmissions. In such dense urban zones, GPS reference stations must often be established on a stationary structure of sufficient height to provide the GPS antenna an ample view of the sky, yet still in close proximity to the rover. It is common practice to neglect lower-elevation satellites, which are inherently noisier, through the use of a mask angle 15° above the horizon. Thus candidate sites for GPS installation must ideally have visibilities from 15 to 90° in elevation on all sides and are generally low- to mid-rise buildings whose own motions are beneath the resolution limits of the GPS sensor (Table 1). The authors were able to successfully isolate a reference building located approximately 0.8 mi (1.29 km) from the monitored rover site, yielding a projected dynamic tracking accuracy of 7.58 mm, according to the expression in Table 1. Though significantly shorter than it surrounding neighbors, resulting in some shielding issues, the selected reference building provides clear views of 70% of the quadrants of the sky.

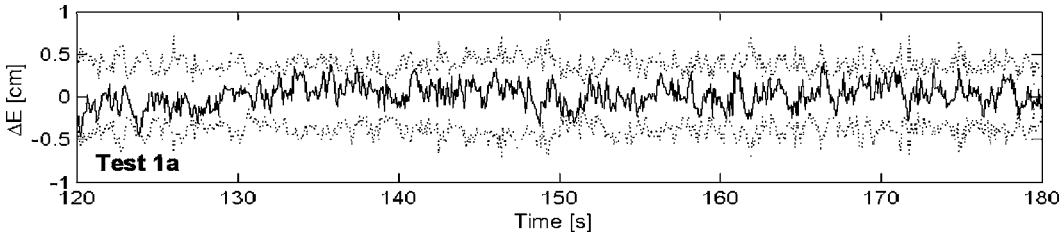

Fig. 6. Example of position quality thresholds (dotted) (cm) superimposed on GPS static displacements (cm) for Test 1a

The GPS units, all supporting electronics and rooftop antennas with rigid galvanized steel mounts were installed at the reference building on August 26, 2002 and at the rover site the following day and continue to be manually triggered to document the displacements of the rover structure during high wind events. Following the sensor placement in Fig. 9 and the electronics configuration in Fig. 2, with the use of traditional telephone lines and a local communications hub in downtown Chicago (Kijewski et al. 2003), the system is remotely operated and data is transmitted to the University of Notre Dame for postprocessing and analysis as described previously. Before the system could be used to determine static deflections of the rover, a baseline position had to be established. As discussed in Tamura (2002), the process involves repeated triggering on calm nights (minimizing dynamic response due to wind and any thermal effects) under high quality DOP conditions. The positions recorded under these conditions are then averaged to establish the baseline position of the rover (X_{E0}, X_{N0}), relative to the local coordinate system, so that true differential displacements can be calculated (ΔE, ΔN), as shown in Fig. 10 (Kijewski-Correa 2005).

Table 6. Summary of GPS Tracking Acccuracy for Simulated Sinusoidal Signals

Sinusoid characteristics	Displacement	ΔN (cm) RMS	ΔN (cm) Minimum	ΔN (cm) Maximum		Noise (cm)
±0.5 cm, 0.1 Hz	GPS	0.38	−0.43	0.37	Δ_{noise}	0.58
	Actual	0.35	−0.49	0.49	x_{max}	0.49
	Errors	7%	−13%	−25%	S/N	85%
±0.5 cm, 1 Hz	GPS	0.37	−0.58	0.49	Δ_{noise}	0.53
	Actual	0.35	−0.48	0.49	x_{max}	0.49
	Errors	5%	21%	1%	S/N	92%
±0.5 cm, 2 Hz	GPS	0.42	−0.56	0.47	Δ_{noise}	0.52
	Actual	0.35	−0.49	0.49	x_{max}	0.49
	Errors	20%	13%	−5%	S/N	95%
±1 cm, 0.1 Hz	GPS	0.68	−0.87	0.82	Δ_{noise}	0.53
	Actual	0.70	−0.99	0.98	x_{max}	0.98
	Errors	−3%	−12%	−18%	S/N	185%
±1 cm, 1 Hz	GPS	0.69	−0.92	0.87	Δ_{noise}	0.50
	Actual	0.71	−1.00	1.00	x_{max}	1.00
	Errors	−2%	−7%	−13%	S/N	198%
±1 cm, 2 Hz	GPS	0.80	−0.86	0.91	Δ_{noise}	0.51
	Actual	0.71	−1.00	1.00	x_{max}	1.00
	Errors	12%	−14%	−9%	S/N	198%
±2 cm, 0.1 Hz	GPS	1.32	−1.99	1.44	Δ_{noise}	0.49
	Actual	1.41	−1.99	1.99	x_{max}	1.99
	Errors	−6%	0%	−28%	S/N	411%
±2 cm, 1 Hz	GPS	1.38	−1.77	2.13	Δ_{noise}	0.50
	Actual	1.41	−1.98	2.00	x_{max}	2.00
	Errors	−3%	−11%	7%	S/N	400%
±3 cm, 0.1 Hz	GPS	1.92	−2.76	2.74	Δ_{noise}	0.77
	Actual	2.12	−2.98	2.98	x_{max}	2.98
	Errors	−9%	−7%	−8%	S/N	384%
±3 cm, 1 Hz	GPS	2.07	−3.13	2.93	Δ_{noise}	0.82
	Actual	2.12	−2.99	2.99	x_{max}	2.99
	Errors	−3%	8%	−2%	S/N	366%

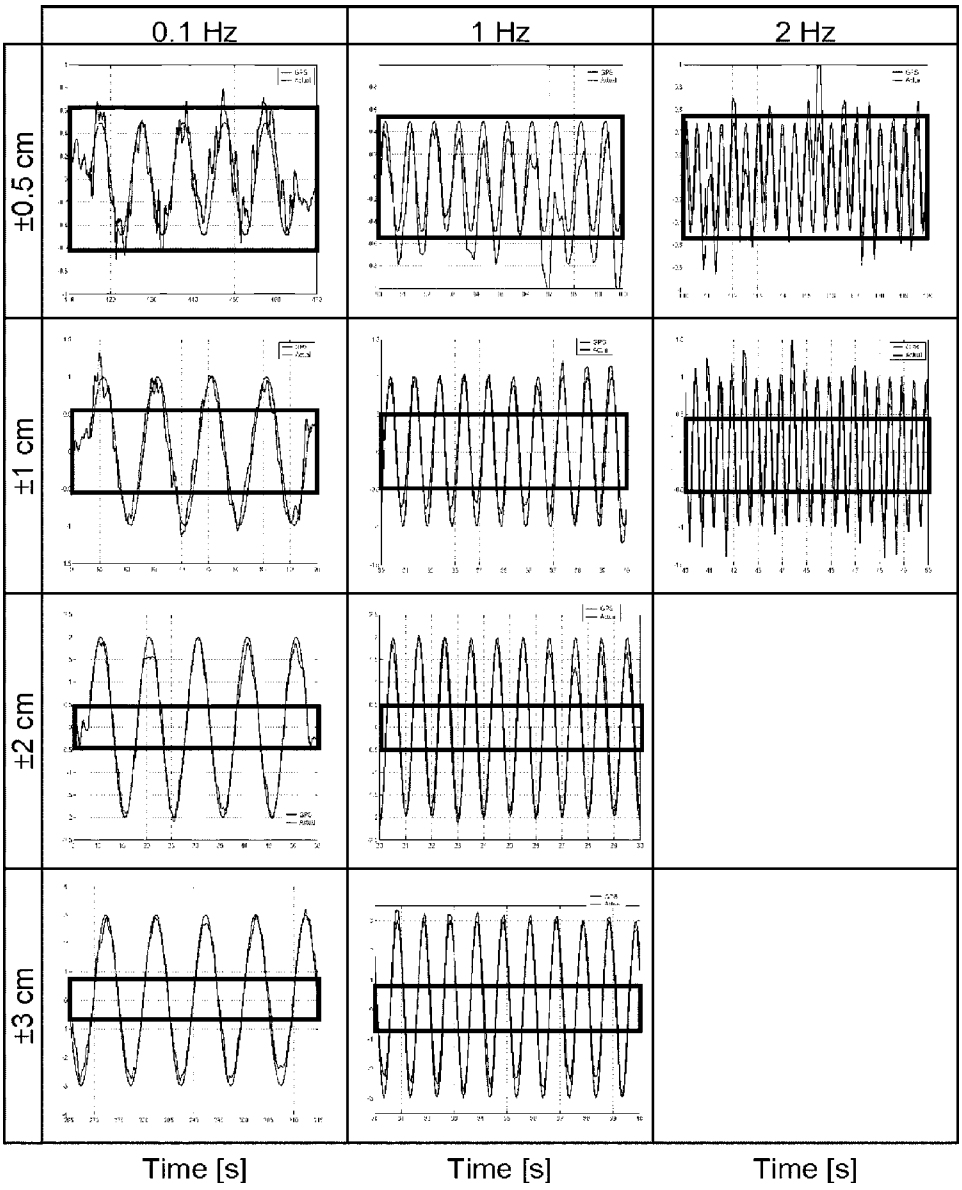

Fig. 7. Comparison of motion simulator displacement (cm) plotted atop GPS displacements (cm) for sinusoidal motions; boxed region indicates mean position quality threshold for that test

Table 7. Summary of GPS Tracking Accuracy for Simulated MDOF Structures under Wind

MDOF system characteristics	Displacement	ΔN (cm) RMS	min	max		Noise (cm)
f_n=0.53 Hz, ξ=0.01	GPS	0.63	−4.27	2.01	Δ_{noise}	0.72
	Actual	0.66	−4.65	2.18	x_{max}	2.18
	Errors	−4%	−8%	−8%	S/N	302%
f_n=0.53 Hz, ξ=0.01	GPS	1.08	−4.79	3.43	Δ_{noise}	0.56
	Actual	1.11	−4.98	3.27	x_{max}	3.27
	Errors	−3%	−4%	5%	S/N	583%
f_n=0.12 Hz, ξ=0.01	GPS	0.91	−2.64	2.32	Δ_{noise}	0.49
	Actual	0.99	−2.63	2.56	x_{max}	2.56
	Errors	−8%	0%	−9%	S/N	518%
f_n=0.12 Hz, ξ=0.01	GPS	1.07	−4.55	2.73	Δ_{noise}	0.52
	Actual	1.14	−5.00	2.76	x_{max}	2.75
	Errors	−6%	−9%	−1%	S/N	527%

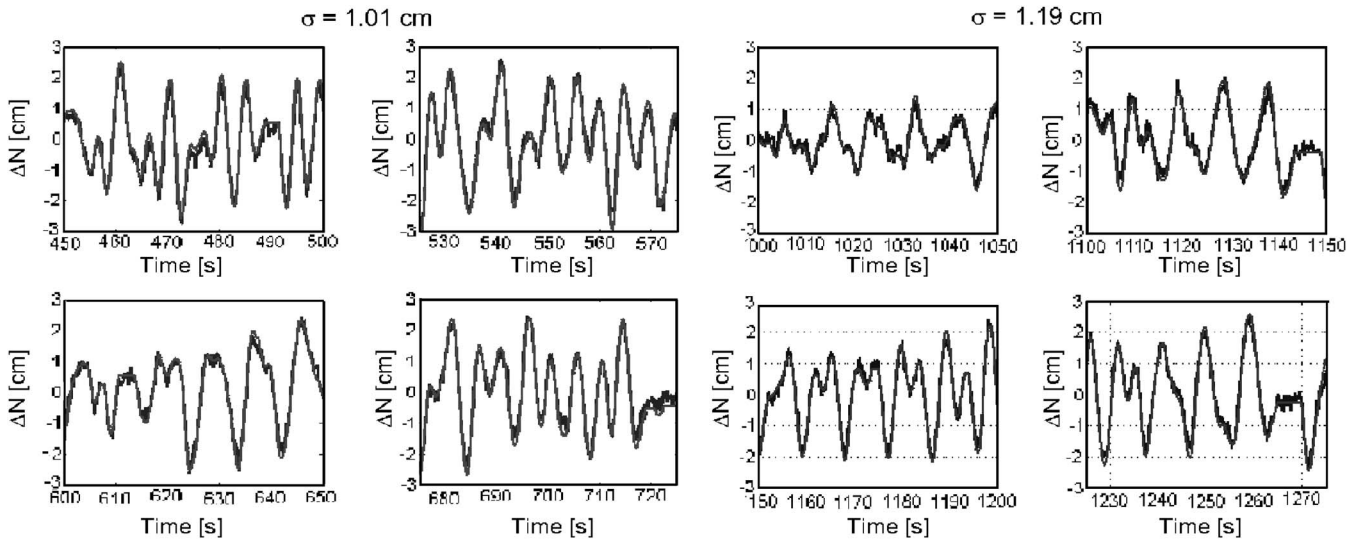

Fig. 8. Snapshots of motion simulator displacement (cm) plotted atop GPS displacements (cm) for simulated MDOF system with f_n=0.12 Hz

Full-Scale Performance Verification

In order to demonstrate the accuracy of the GPS sensors in full scale, comparisons to the accelerations recorded in the rover structure through its primary instrumentation system have been conducted, an example of which is now presented for a wind event that occurred on November 24, 2003. During this event, winds approached from the West-Northwest (283–290°) to produce predominantly alongwind response in the rover's N-S axis. The winds recorded at the surface of Lake Michigan by a NOAA instrumentation station were 14–16 m/s for the data presented herein, producing estimated rooftop wind speeds of 18.7–21.3 m/s (Kochly et al. 2005). Through the use of bandpass filters, the comparisons presented here are restrained to the dominant fundamental sway responses along the N-S and E-W axes of the building. GPS displacements were converted to accelerations by a double differencing approach. A comparison of the measured accelerations at full-scale to the GPS-derived accelerations are provided in both the time and frequency domains in Fig. 11 and show an excellent correlation between the sensors, further affirmed by the calculated RMS accelerations in Table 8. Note that additional full-scale comparisons of accelerometers to GPS have been conducted for other wind events as discussed in Kijewski-Correa et al. (2006) and Kochly and Kijewski-Correa (2005) and have similarly found excellent agreement between the two sensor technologies for capturing resonant response. The latter study and additional work by Kochly et al. (2005) then extended the evaluation of GPS to consider the correlations between its measured background component and that predicted by wind tunnel testing to emphasize the variability in predicted responses and the role of multipath effects in distorting measurements of background response.

Full-Scale Displacement Data

An analysis of the total displacements in the November 24, 2003 wind event is now presented. As discussed in Kochly et al. (2005) and previously in this paper, the issues of multipath interference are still very much of concern for installations of GPS in urban zones. This residual error source in GPS monitoring induces long period distortions in the calculated displacement estimates that

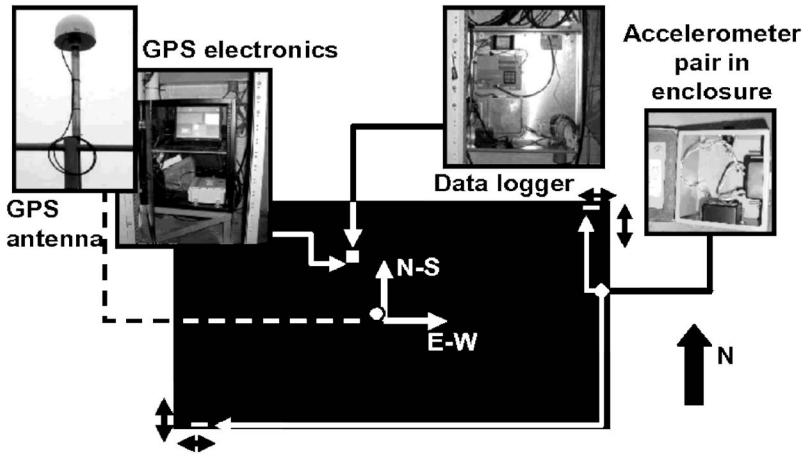

Fig. 9. Schematic of response instrumentation in building housing GPS rover in conjunction with Chicago full-scale monitoring program (dashed lines indicate rooftop installation, solid lines indicate installation at highest mechanical floor)

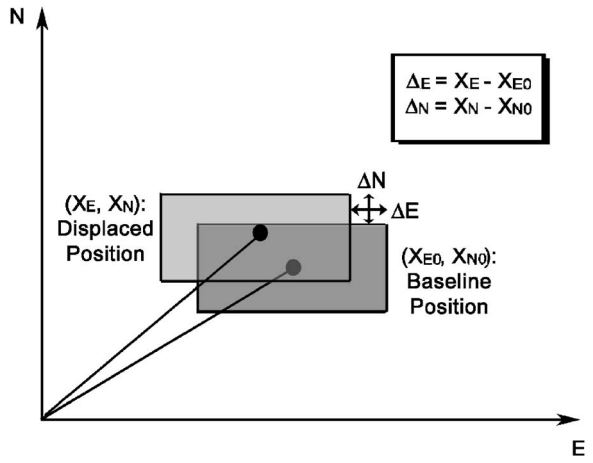

Fig. 10. Schematic representation of relative displacements defined with respect to structural baseline in local coordinate system

can interfere with the ability to accurately determine background wind-induced response. Removal by traditional bandstop filtering (Kochly et al. 2005) or wavelet-based decomposition (Chen et al. 2001) has shown some utility, though further advancements in receiver hardware and software show even greater promise in removing multipath distortions directly in the solution for GPS displacements. Nevertheless, the filtering approach discussed in Kochly et al. (2005) is now applied, resulting in the two-dimensional building response plot shown in Fig. 12. Note that the displacement response is dominantly acrosswind for this event with a large resonant response along the N-S building axis, which has a fundamental frequency that is 40% softer than its alongwind counterpart. The associated background, resonant and total response time histories, and the power spectral density of the total response are shown in Fig. 13. As expected, the resonant response component of the N-S axis is significantly larger than the E-W due to the dominance of the acrosswind motions. It is also important to note that despite the E-W axis being the alongwind response direction, which would generally be expected to have the larger background response component, the background component of the acrosswind response is still larger, again due to the disproportionate stiffness along these two building axes.

Table 8. Comparison of RMS Acceleration Values in Full Scale by Accelerometer and GPS for Response in Fundamental Mode

Response component	Full-scale accelerometers (mg)	Full-scale GPS (mg)	Percent deviation from accelerometer
E-W	0.35	0.35	0.00
N-S	1.02	0.96	6.40

Assessment of Performance in Full Scale

The GPS pair prototyped and calibrated in this study has been in operation now for several years, over which period their performance in full-scale has been evaluated. Moving into dense urban environments, issues of radio frequency (RF) interference, and other noise sources become concerning. To date, there has been no loss of tracking ability due to RF interference, though at times a solution for GPS displacements cannot be achieved satisfactorily, leading to lesser reliability of displacement predictions due to elevated DOP levels. This is a result of the blockage of

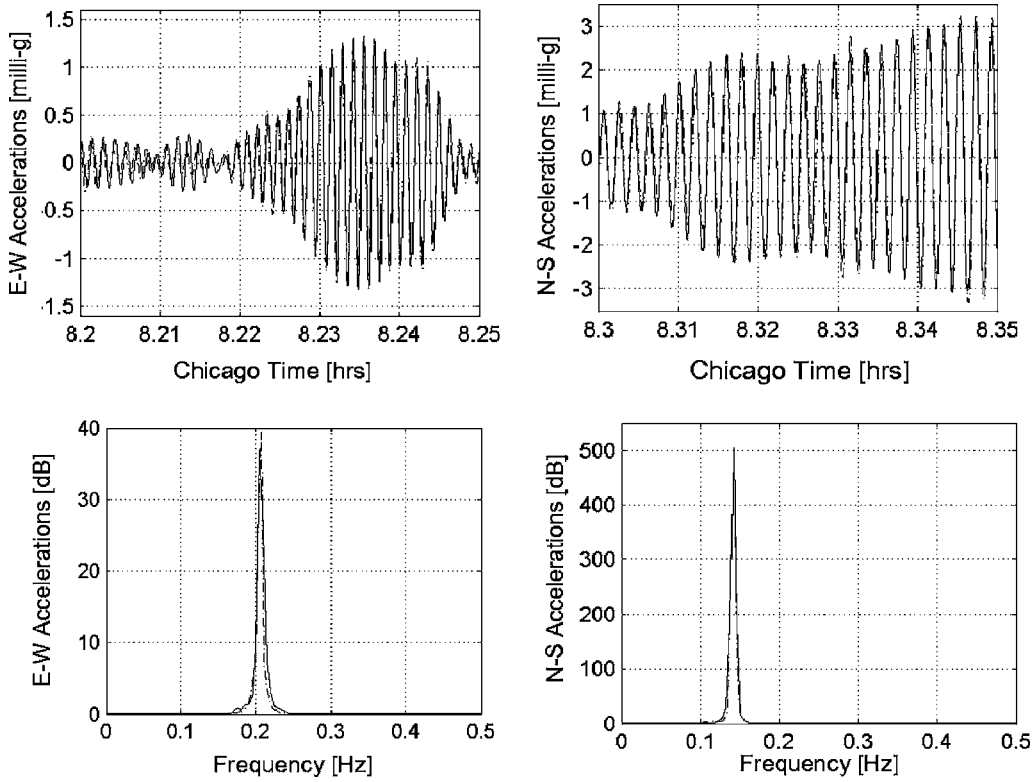

Fig. 11. Zoom of accelerometer data (dashed) plotted atop of GPS-derived accelerations (dotted) for November 24, 2003 wind event, with power spectral density shown below

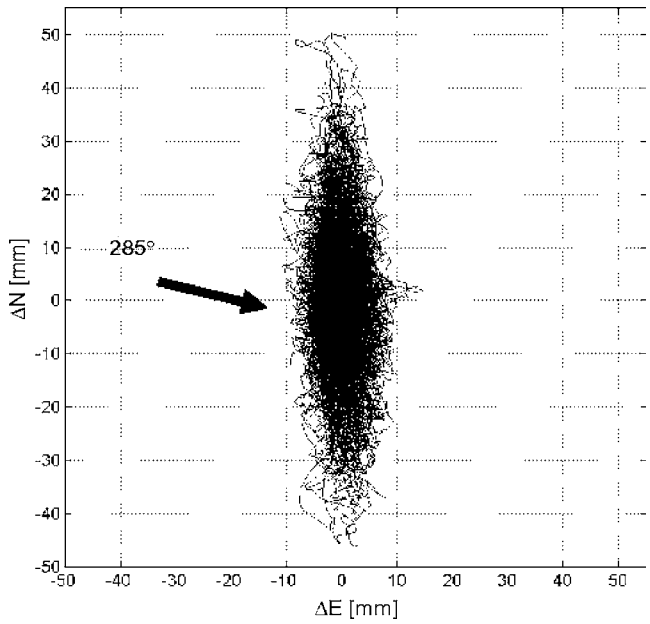

Fig. 12. Two-dimensional plot of GPS displacements during November 24, 2003 wind event, with arrow indicating average wind direction

satellites at the shorter reference structure, where at times only 4–5 satellites may be in view, in comparison with the taller rover, which can track eight or more satellites at a given time. When the constellation at the reference site further degrades to less than four satellites, GPS positions can no longer be determined via Eq. (2) and there is a temporary loss of tracking until the satellite configuration repopulates at higher elevations. The impacts of satellite loss and the use of PQTs in diagnosing the root causes of degraded measurements in full scale are demonstrated in Kijewski-Correa and Kareem (2003). The continuous performance of the full-scale deployment here can be reasonably enhanced simply by moving the reference site to a less shielded location on the west side of the city, an option currently being explored in conjunction with Leica Geosystems.

The PQTs observed in full scale are elevated in comparison to those determined through calibration studies, as expected in light of the lengthened baselines and increased interference sources (Kijewski-Correa and Kareem 2003). Though this finding was by no means alarming, this situation does require motions of the building to be on the order of a few centimeters for peak responses to be reliably tracked. Clearly, however, the issues of multipath effects remain the most prominent error source in the deployment of GPS for structural monitoring in urban zones. Their effects have been noted by a number of researchers, e.g., Lovse et al. (1995), Chen et al. (2001), and Kochly et al. (2005), and have motivated the introduction of a new program by the first author including a series of controlled multipath tests to identify and effectively remove these systematic errors through time series strategies that better preserve the background response (Kijewski-Correa et al. 2004).

Conclusions

The present study discusses the use of high-precision global positioning systems for monitoring the displacement of tall buildings under the action of wind, providing the opportunity to monitor mean and background components of wind-induced response that cannot be recovered from accelerometers. Prior to the deployment of a GPS pair in the City of Chicago, as part of a larger full-scale monitoring program, the authors conducted extensive field calibration studies. In the context of this calibration program, the authors introduced the new concept of PQTs to provide end users with a means to estimate the level of background noise in GPS measurements at full scale. It was demonstrated in the dynamic calibration testing that reliable tracking of RMS response could be achieved when the effective peak signal-to-noise ratio, calculated using these PQTs, was 200% or more, generally corresponding to motions above ±1 cm. Meanwhile, errors in

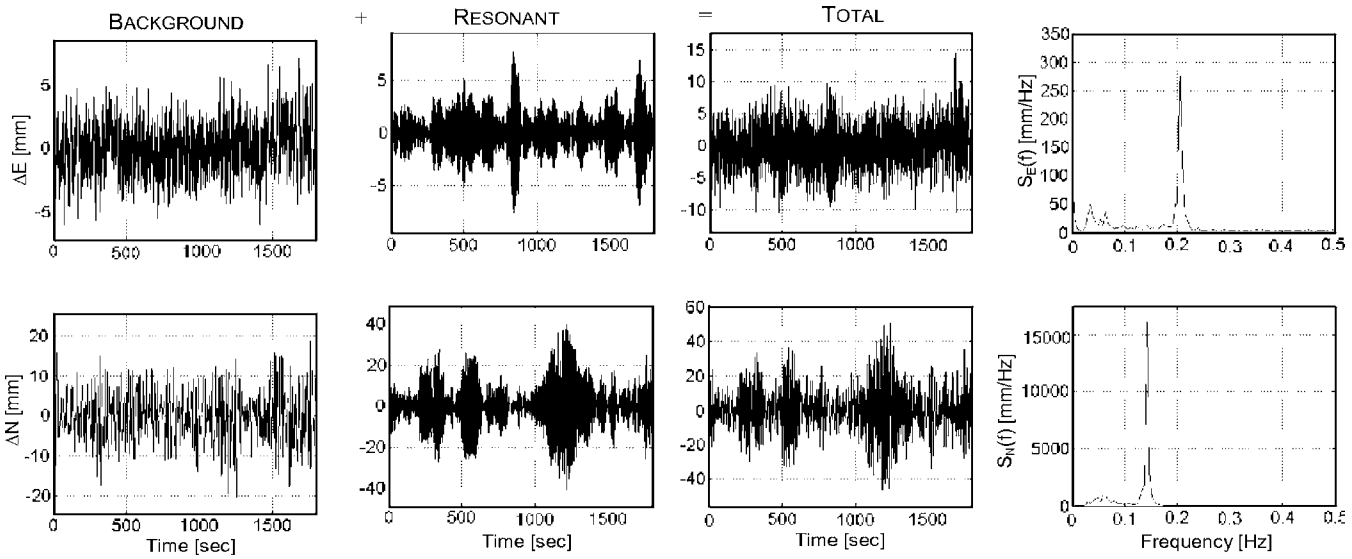

Fig. 13. GPS response for November 24, 2003 wind event: background, resonant, and total displacements, with power spectral density of total displacements at far right

peak estimation are consistently mitigated for signals with amplitudes above ±2 cm. The calibration program also demonstrated that at sufficiently large amplitudes, GPS performance is independent of the frequency of motion, however, for low amplitude motions, tracking is superior at lower frequencies, further motivating its application to the monitoring of flexible Civil structures. This was further demonstrated in the tracking of simulated motions of tall buildings under the action of wind, where GPS performance produced tracking errors of less than 10%. The authors then discussed the full-scale deployment of the system on a tall building in Chicago, demonstrating the excellent correlation between GPS and accelerometers in dynamic response tracking. In light of the ongoing analysis of data from this program and a second stage of multipath testing and removal, this study affirms the promise of GPS as a highly reliable sensor for monitoring total structural displacements, not only under the action of wind, but also the static displacements associated with settlement, thermal expansion or permanent offsets resulting from damaged states. This potential will only be enhanced in the coming years with hardware advancements and as more GPS satellites become available through the launching of other international satellite systems to reduce DOP errors even further.

Acknowledgments

The writers are grateful for the financial support of the National Science Foundation, via Grant No. CMS 00-85109, and the University of Notre Dame. They also wish to acknowledge their collaborators on the project: the Boundary Layer Wind Tunnel Laboratory at the University of Western Ontario and Skidmore Owings and Merrill LLP in Chicago, as well as Dr. Dae Kun Kwon, NatHaz post-doctoral research assistant, and Ms. Lijuan Wang and Ms. Tiphaine Williams, graduate students from the University of Notre Dame. Of course, this project would not be possible without the cooperation and assistance of the building owners and management at the reference and rover sites—the support and enthusiasm of all the participants is gratefully acknowledged. Thanks also go to Mr. John Berkebile of the St. Joseph Co. Ind. Parks Department for assistance in the GPS calibrations and to Mr. James Stowell and his staff at Leica Geosystems for their technical counsel and generous support of this program.

References

Axelrad, P., Comp, C. J., and Macdoran, P. E. (1996). "SNR-based multipath error correction for GPS differential phase." *IEEE Trans. Aerosp. Electron. Syst.*, 32(2), 650–659.

Brownjohn, J. M. W. (2003). "Sensor and data management technology for structural health monitoring of civil structures." *Proc., Structural Health Monitoring and Intelligent Infrastructure*, Swets & Zeitlinger, Lisse, The Netherlands, 1235–1242.

Celebi, M. (2000). "GPS in dynamic monitoring of long-period structures." *Soil Dyn. Earthquake Eng.*, 20, 477–483.

Celebi, M., and Sanli, A. (2002). "GPS in pioneering dynamic monitoring of long-period structures." *Earthquake Spectra*, 18(1), 47–61.

Chan, W. S., Xu, Y. L., Ding, X. L., Xiong, Y. L., and Dai, W. J. (2005). "Dynamic displacement measurement accuracy of GPS for monitoring large civil engineering structures." *Proc., SPIE Int. Symp. on Smart Structures and Nondestructive Evaluation* (CD-ROM), SPIE, Bellingham, Wash.

Chen, Y., Huang, D., Ding, X., Xu, Y., and Ko, J. M. (2001). "Measurement of vibrations of tall buildings: a case study." *Proc., SPIE Conf. on Nondestructive Evaluation* (CD-ROM), SPIE, Bellingham, Wash.

Counselman, C. C. (1999). "Multipath-rejecting GPS antennas." *Proc. IEEE*, 87(1), 86–91.

Guo, J., and Ge, S. (1997). "Research of displacement and frequency of tall building under wind load using GPS." *Proc., 10th Int Technical Meeting of the Satellite Division of the U.S. Institute of Navigation*, Kansas City, Mo., 1385–1388.

Kareem, A., and Kijewski-Correa, T. (2002). "Chicago full-scale monitoring program." ⟨http://windycity.ce.nd.edu⟩.

Kijewski, T., and Kareem, A. (2002). "GPS for monitoring the dynamic response of tall buildings." *Proc., Structures Congress* (CD-ROM), ASCE, Reston, Va.

Kijewski, T., Kwon, D. K., and Kareem, A. (2003). "E-Technologies for wind effects on structures." *Proc., 11th Int. Conf. on Wind Engineering* (CD-ROM), Texas Tech Univ., Lubbock, Tex.

Kijewski-Correa, T. (2003). "Full-scale measurements and system identification: A time-frequency perspective." Ph.D. dissertation, Univ. of Notre Dame, Notre Dame, Ind.

Kijewski-Correa, T. (2005). "GPS: a new tool for structural displacement measurement." *APT Bull.*, 36(1), 13–18.

Kijewski-Correa, T., and Kareem, A. (2003). "The height of precision." *GPS World*, 13(9), 20–34.

Kijewski-Correa, T., Kochly, M., and Stowell, J. (2004). "On the emerging role of GPS in structural health monitoring." *Proc., CTBUH 2004*, Hanrimwon, Seoul, Korea, 144–151.

Kijewski-Correa, T. et al. (2006). "Validating the wind-induced response of tall buildings: a synopsis of the Chicago full-scale monitoring program." *J. Struct. Eng.*, in press.

Kochly, M., and Kijewski-Correa, T. (2005). "Monitoring tall buildings under the action of wind: the role of GPS in urban zones." *Proc., 4th European and African Conf. on Wind Eng.* (CD-ROM), Czech Technical Univ., Prague, Czech Republic.

Kochly, M., Kijewski-Correa, T., and Stowell, J. (2005). "GPS for monitoring in urban zones: calibration and quantification of multipath effects." *Proc., SPIE Conf. on Smart Structures and Materials/NDE for Health Monitoring and Diagnostics* (CD-ROM), SPIE, Bellingham, Wash.

Leica. (1999a). *Introduction to GPS v. 1.0*, Leica Geosystems, Heerbrugg, Switzerland.

Leica. (1999b). *Technical specifications of Leica GPS system 500*, Leica Geosystems, Heerbrugg, Switzerland.

Lovse, J. W., Teskey, W. F., Lachapelle, G., and Cannon, M. E. (1995). "Dynamic deformation monitoring of tall structure using GPS technology." *J. Surv. Eng.*, 121(1), 35–40.

Park, H. S., Shon, H. G., Kim, I. S., and Park, J. H. (2004). "Monitoring of structural behavior of high-rise buildings using GPS." *Proc., CTBUH 2004*, Hanrimwon, Seoul, Korea, 1064–1071.

Seeber, G. (1993). *Satellite geodesy—foundations, methods and applications*, Walter de Gruyter, Berlin.

Tamura, Y. (2002). "Dynamic monitoring response of structures using GPS." *Proc., ASCE Structures Congress* (CD-ROM), ASCE, Reston, Va.

Tamura, Y., Matsui, M., Pagnini, L.-C., Ishibashi, R., and Yoshida, A. (2002). "Measurement of wind-induced response of buildings using RTK-GPS." *J. Wind. Eng. Ind. Aerodyn.*, 90, 1783–1793.

Tranquilla, J. M., Carr, J. P., and Al-Rizzo, H. M. (1994). "Analysis of a choke ring groundplane for multipath control in global positioning system (GPS) applications." *IEEE Trans. Antennas Propag.*, 42(7), 905–911.

Van Nee, R. D. J. (1995). "Multipath and multi-transmitter interference in spread-spectrum communication and navigation systems." Thesis, Delft University of Technology Press, Delft, The Netherlands.